

Coalescence cascade of dissipative solitons in parametrically driven systems

M. G. Clerc,¹ S. Coulibaly,² L. Gordillo,¹ N. Mujica,¹ and R. Navarro¹

¹*Departamento de Física, Facultad de Ciencias Físicas y Matemáticas, Universidad de Chile, Casilla 487-3, Santiago, Chile*

²*Laboratoire de Physique des Lasers, Atomes et Molécules, CNRS UMR 8523, Université des Sciences et Technologies de Lille—59655 Villeneuve d'Ascq Cedex, France, EU*

(Received 23 March 2011; published 8 September 2011)

Parametrically driven spatially extended systems exhibit uniform oscillations which are modulationally unstable. The resulting periodic state evolves to the creation of a gas of dissipative solitons. Driven by the interaction of dissipative solitons, the multisoliton state undergoes a cascade of coalescence processes, where the average soliton separation distance obeys a temporal self-similar law. Starting from the soliton pair interaction law, we have derived analytically and characterized the law of this multisoliton coarsening process. A comparison of numerical results obtained with different models such as the parametrically driven damped nonlinear Schrödinger equation, a vertically driven chain of pendula, and a parametrically forced magnetic wire, shows remarkable agreement. Both phenomena, the pair interaction law and the coarsening process, are also observed experimentally in a quasi-one-dimensional layer of Newtonian fluid which is oscillated vertically.

DOI: [10.1103/PhysRevE.84.036205](https://doi.org/10.1103/PhysRevE.84.036205)

PACS number(s): 47.54.-r, 05.45.Yv, 05.45.-a

I. INTRODUCTION

An outstanding property in many nonequilibrium systems is their ability to generate coherent spatiotemporal structures or patterns [1–4], which arise from a balance between dissipation and energy injection. Despite the physical differences of these systems, particularly from a microscopic point of view, the dynamics of the pattern belongs to the same universality class. Thus, one can understand the interest to create and develop tools that allow an unified description, such as amplitude equations. These consist basically in a reduction from more basic and complex equations. Starting from microscopic equations of motion, equations from first principles, or phenomenological models describing a given physical system, one can obtain a simpler macroscopic dynamical system that accounts for the emergence of the pattern. In the past decades, major efforts have been made to characterize these type of equations. However, to the best of our knowledge, there is still no comprehensive global characterization. Among the most known classes of amplitude equations are Ginzburg-Landau [5], Korteweg-de Vries (KdV) [6], Swift-Hohenberg [4,7], nonlinear Schrödinger (NLS) [8], and so forth. All these models have been used to describe different phenomena in diverse areas such as fluid dynamics, optics, chemical reactions, magnetism, electricity, liquid crystals, biology, crystal growth, population dynamics, astrophysics, geophysics, engineering, shell patterns, fur of mammals and insects, etc. (see Refs. [2–4,9,10] and references therein).

On the other hand, to maintain nonequilibrium systems one must consider the injection of energy by forcing. The response of a dynamic system to such energy injection is strongly related to the dynamic nature of the system under study, particularly to its intrinsic frequencies. The two most prominent mechanisms are synchronization [11] and resonance phenomenon [12]. The 1:1 resonance, which is also known as *simple* resonance, occurs when energy is directly injected into the system in such a way that response and forcing have the same frequency [12]. When the driving is applied by modulating the parameters describing the system, the resonance is called *parametric*. The

system responds to the forcing with oscillations in different frequencies. A classic example of this behavior is Faraday waves [13,14], where the system responds at half the forcing frequency (2:1 resonance). Experimental examples of this phenomenon have been reported in nonlinear optics, classical mechanics, magnetodynamics and so forth.

A chain of one-degree-of-freedom nonlinear oscillators under 2:1 resonance is well described by the parametrically driven damped nonlinear Schrödinger equation [14,15], which corresponds to a variant of the nonlinear Schrödinger equation. Spatially extended systems under parametric excitation have been reported to exhibit periodic patterns (triangles, hexagons, rolls, and so forth) [16–18], localized structures (dissipative soliton, fronts, kinks, localized states) [14,15,19–21], propagative domain walls [22], and many other structures. The study of localized states—which correspond to particle-type solutions—in parametric processes keeps attracting great interest in all the aforementioned physical areas, not only from a fundamental point of view, but from an applied perspective as well. The most studied localized state is the nonpropagative soliton [15]. It can be observed near the parametric resonance when a weak damping and driving strength are considered, as it occurs in the quasireversible limit [23]. This solution rises through a saddle-node bifurcation [15,24]. Then, it can be formed only if the localized perturbation lies on its basin of attraction. Furthermore, the dissipative soliton coexists with a stable quiescent state (zero uniform state) and nonzero homogeneous state, which is unstable to cnoidal waves [25]. In fact, after a given time, the cnoidal wave periodicity is broken and neighbor peaks exhibit an attractive interaction that ends with the emergence of a single one.

Then, a cascade of neighbor coalescing peaks follows, leading to the formation of a stable multisoliton state, and also to the spontaneous formation of solitary structures. The above process can be observed in a region of parameters similar to that on which solitons can be found [26]. Figures 1(a)–1(c) show, respectively, coalescence processes for three prototype models of parametric systems: the parametrically driven damped nonlinear Schrödinger equation, a parametrically

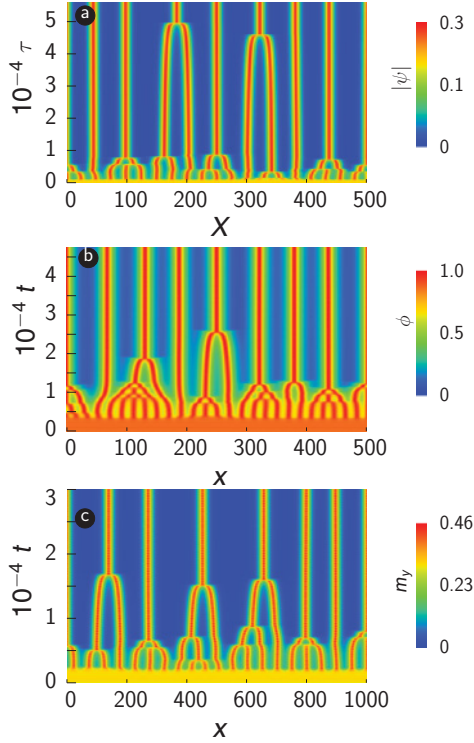


FIG. 1. (Color online) Cascade of coalescence processes observed numerically in (a) the parametrically driven damped nonlinear Schrödinger equation ($\mu = 0.050$, $\gamma = 0.053$, $\nu = -0.03$), (b) a parametrically vertically driven pendula chain ($\mu = 0.100$, $\gamma = 0.212$, $\nu = -0.030$), and (c) easy-plane ferromagnetic spin chain exposed to a periodic external field ($H = 0.200$, $h = 0.044$, $\beta = 4.800$, $\alpha = 0.020$, $\nu = -0.030$).

vertically driven pendula chain, and an easy-plane ferromagnetic spin chain exposed to a periodic external field.

In this paper, we are concerned with the characterization of the above coarsening process, particularly in the evolution in time of the average separation distance of solitons. The processes depicted in Fig. 1 serve as evidence of the universality of the coalescence process in parametrically driven systems. In order to provide a unified description of this phenomenon, we consider the amplitude equation that accounts for these type of systems as the starting point. Figure 1 also shows clearly that the cascade coalescence process is mediated by the interaction of soliton pairs. Thus, one can assume that the statistical dynamics is lead by the soliton-soliton interaction. From the analytical characterization of the soliton pair interaction and its subsequent experimental verification in a vertically forced water channel, we infer the coarsening law which controls the coalescence cascade.

The paper is organized in the following way: Section II gives the guidelines for derivation of the amplitude equation of nonlinear oscillators under parametric excitation. The pair interaction law is characterized in Sec. III. In this section we also highlight our experimental evidence of this law and report multisoliton coalescence processes as well. In Sec. IV, we model the behavior of a gas of *diluted* solitons. Finally, conclusions and remarks are presented in Sec. V.

II. GENERIC MODEL OF PARAMETRIC INSTABILITY: THE PARAMETRICALLY DRIVEN DAMPED NONLINEAR SCHRÖDINGER EQUATION

Parametric resonance is an instability phenomenon [27], which offers entire control of the system by means of the driving *strength*. Thus, numerous examples of this type of forced oscillator can be counted from classical mechanics to quantum mechanics through hydrodynamics and optics. For an extended oscillator under 2:1 resonance, the envelope of the oscillation is described by the complex field $\psi(X, \tau)$. At dominant order, this order parameter satisfies the dimensionless parametrically driven damped nonlinear Schrödinger equation [14,15]

$$\partial_\tau \psi = -i\nu\psi - i|\psi|^2\psi - i\partial_X^2\psi - \mu\psi + \gamma\bar{\psi}, \quad (1)$$

where $\{\tau, X\}$ account for time and space, respectively, and the parameters $\{\nu, \mu, \gamma\}$ stand for the detuning between the natural and half the forcing frequency, the damping, and the intensity of the forcing, respectively. The parameters that control the resonance are the detuning and the intensity of the forcing. Near resonance, the detuning is a small parameter ($\nu \ll 1$) and the above amplitude equation is valid in the following, scaling $\psi \sim \nu^{1/2}$, $\mu \sim \gamma \sim \nu$, $\partial_X \sim \nu^{1/2}$, and $\partial_\tau \sim \nu$. Hence, the terms in Eq. (1) are of order $\nu^{3/2}$. Higher-order terms were neglected. The term proportional to ν describes the difference between the forcing frequency and twice the natural frequency. The nonlinear term accounts for the nonlinear response of the oscillation envelope as a function of its own amplitude and its negative sign is linked to the soft nature of the oscillator. The term with spatial derivatives accounts for the dispersive effect of the original system, which, together with the nonlinearity, characterizes the focusing features of the system. The terms proportional to μ and γ describe, respectively, linear dissipation and energy injection through a parametric forcing of the 2:1 type. Examples of systems modeled by Eq. (1) include vertically oscillating fluid layers [14,26], nonlinear lattices [28], optical fibers [29], Kerr-type optical parametric oscillators [19], magnetization in easy-plane ferromagnetic materials subject to periodic magnetic fields [21,30], and a vertically driven damped chain of pendula [31].

It is noteworthy that model (1) has played a central role in understanding the formation of patterns and dissipative solitons in parametrically forced systems. However, this model does not contain stable nonzero uniform states, which account for uniform oscillations which can be trapped by considering corrections of this model [20,21]. These terms help to explain other localized states observed in parametrically driven systems.

With the aim of emphasizing the widespread nature of the phenomenon under study, we consider two different physical systems, a vertically driven pendula chain and a classical easy-plane ferromagnetic spin chain. Since the derivation of Eq. (1) is detailed in the references cited above, we will discuss only the relation between the dimensionless parameters and variables of this equation with the original physical systems.

A vertically driven pendula chain. In the continuum limit, a vertically driven pendula chain in a viscous medium with

an elastic nearest-neighbor coupling is well described by the driven and damped sine-Gordon equation:

$$\ddot{\phi}(x,t) = -[\omega_0^2 + \Gamma \sin(\omega t)] \sin(\phi) - \alpha \dot{\phi} + k \partial_{xx} \phi, \quad (2)$$

where $\phi(x,t)$ is the angle formed by the pendulum and the vertical axis at the x position at time t . ω_0 is the pendula natural frequency and the parameters $\{\alpha, k, \Gamma, \omega\}$ are the damping, elastic coupling, amplitude, and frequency of the parametric forcing, respectively. We now choose the forcing frequency ω to be close to twice the natural frequency ω_0 . Indeed, if one assumes a weak forcing and damping—quasireversible limit—the solution of the small deviation angles is well described by the following ansatz:

$$\begin{aligned} \phi(x,t) = & 2\sqrt{\frac{\varepsilon}{\omega_0}} \psi(X,\tau) e^{i(\omega_0+\nu)t} - 2\sqrt{\frac{\varepsilon}{\omega_0}} \left\{ \frac{\psi^3(X,\tau)}{48} \right. \\ & + \frac{i\gamma}{16\omega_0^2} \psi(X,\tau) - \frac{i\gamma\varepsilon}{8\omega_0^3} |\psi(X,\tau)|^2 \psi(X,\tau) \left. \right\} e^{3i(\omega_0+\nu)t} \\ & + \text{c.c.} + \text{h.o.t.}, \end{aligned} \quad (3)$$

where $\tau = \varepsilon t$, $X = \sqrt{2\varepsilon\omega_0/k}x$, and ε is a small parameter measuring the distance to the parametric resonance such that $\Gamma \sim \alpha \sim \nu \sim \varepsilon$. Combining both Eqs. (2) and (3), and assuming $\theta \ll 1$, this is $\sin(\theta) \simeq \theta - \theta^3/3$, the solvability condition that yields to Eq. (1) after setting $\nu = \omega/2 - \omega_0$, $\gamma = \Gamma/4$, and $\mu = \alpha/2$. Therefore, the envelope of the oscillation of the vertically driven pendula chain in the quasireversible limit is described by the model (1).

A *classical easy-plane ferromagnetic spin chain*. In the continuum approximation limit, in which the relative position of two neighbor spins or magnetic moments displays only a slight variation, a one-dimensional wire of easy-plane ferromagnetic material such as CcNiF_3 or $\text{Ni}_{80}\text{Fe}_{20}$ is described by the well-known Landau-Lifshitz-Gilbert equation, which in dimensionless form is written as [30,32]

$$\begin{aligned} \partial_t \mathbf{M} = & \mathbf{M} \times \mathbf{M}_{xx} - \beta(\mathbf{M} \cdot \hat{x})(\mathbf{M} \times \hat{x}) + \mathbf{M} \times \mathbf{H} \\ & - \alpha \mathbf{M} \times \mathbf{M}_t, \end{aligned} \quad (4)$$

where $\mathbf{M}(x,t)$ stands for the normalized unit vector of the magnetization along the direction of the wire which is represented by the coordinate x and $\beta > 0$ is the easy-plane anisotropy constant. Thus, magnetization minimizes the magnetic energy when it is orthogonal to the wire. $\hat{x} \equiv (1,0,0)$ denotes the unit vector along the *hard axis*, α is the relaxation constant, and $\mathbf{H} \equiv (0,0,H)$ is an applied magnetic field orthogonal to the wire. Under the influence of a constant external field [$H(t) = H(0) = H_0$], any spin perturbation along the chain go through a damped gyroscopic precession to the stable state, which corresponds to the spins aligned with the field [21]. The frequency of this precession is given by $\omega_0 \equiv \sqrt{H_0(\beta + H_0)}$. Hence, model (4) describes a chain of nonlinear oscillators characterized by (a) the conservation of magnetization modulus and (b) the alignment of magnetization with the external field.

In the case of considering H having both constant H_0 and time-dependent $h_1(t)$ components, such that $h_1 \ll H_0$ accounts for small deviations of the magnetization with respect to the direction of the constant external field $H_0 \hat{z}$ [$\hat{z} \equiv (0,0,1)$],

the set of three equations (4) can be reduced to a single one [21]:

$$\begin{aligned} \ddot{m}_z = & -[\omega_0^2 - (\beta + 2H_0)h_1] m_z + (\beta + 2H_0) \partial_{zz} m_z \\ & - \frac{\beta + 2H_0}{2} \alpha \dot{m}_z - \frac{\dot{h}_1}{H_0} \dot{m}_z + \frac{\beta}{2H_0} (\dot{m}_z^2 + H_0^2 m_z^2) m_z, \end{aligned} \quad (5)$$

where m_z is the component of magnetization in the direction \hat{z} . The upper dots represent derivatives with respect to the time. The above model stands for a parametrically forced mechanical extended oscillator. The other components of the vector \mathbf{M} are related to m_z at dominant order as follows:

$$m_x \simeq 1 - \frac{m_y^2 + m_z^2}{2}, \quad (6)$$

$$m_y \simeq -\frac{1}{H_0} \left(1 + \frac{h_1}{H} \right) \partial_t m_z. \quad (7)$$

When $h_1(t)$ oscillates harmonically close to twice the natural frequency ω_0 , the forced magnetic wire exhibits a parametric resonance. Introducing the following ansatz,

$$m_z = 4 \sqrt{\frac{\omega_0 H_0}{\beta(\omega_0^2 + 3H_0^2)}} \text{Re}(\psi e^{i(\omega_0+\nu)t}) + w(x,t,\psi), \quad (8)$$

in Eq. (5) and linearizing the small corrections $w(x,t,\psi)$, the solvability condition for the amplitude of the oscillations leads to Eq. (1) with $X \equiv \sqrt{2\omega_0/(\beta + 2H_0)}x$, $\mu \equiv (\beta + 2H_0)\alpha/2$, and $\gamma \equiv \beta h/4\omega_0$. Notice that for a high anisotropy regime ($\beta \gg H$), Eq. (4) can be reduced to Eq. (2) after setting $\omega_0^2 \equiv H_0\beta$, $\Gamma \equiv \beta h$, $\mu \equiv \beta\alpha$, $k \equiv \beta$, and ϕ being the azimuthal angle in the easy plane [30,33].

In brief, a vertically driven pendula chain and a classical easy-plane ferromagnetic spin chain show the same type of behavior near the parametric resonance, which is described by the amplitude equation (1).

III. NONLINEAR WAVE COLLAPSE AND NONPROPAGATIVE SOLITON INTERACTION

When the detuning is negative ($\nu < 0$), Eq. (1) has nontrivial exact steady *solitonic* solutions of the form [30]

$$\cos(2\theta_0) = \frac{\mu}{\gamma}, \quad (9a)$$

$$R_{\pm}^0(X) = \sqrt{2} \delta_{\pm} \text{sech}(\delta_{\pm}[X - X_0]), \quad (9b)$$

where $\delta_{\pm} = \sqrt{-\nu - \gamma \sin(2\theta_0)} = \sqrt{-\nu \pm \sqrt{\gamma^2 - \mu^2}}$ such that $\psi(X,\tau) \equiv \psi_{\pm}(X) = \chi R_{\pm}(X) e^{i\theta_0}$. Thus, these solitons are completely characterized by two related parameters, amplitude ($\sqrt{2}\delta_{\pm}$) and width (δ_{\pm}^{-1}), the phase θ_0 that is fixed by the balance between injection and dissipation of energy, plus two others arbitrary parameters, the position (X_0) linked to spatial translation symmetry displayed by Eq. (1) and the *polarity* ($\chi = \pm 1$, hence this is a sign parameter). ψ_+ solutions are stable only when $\mu < \gamma < \sqrt{\mu^2 + \nu^2}$ with small detuning. In this region the soliton coexists with the quiescent state $\psi_0 = 0$. As it is shown in the bifurcation diagram (Fig. 2), the soliton rises through a saddle-node bifurcation with respect to the driving strength γ at fixed ν and μ . Consequently, it

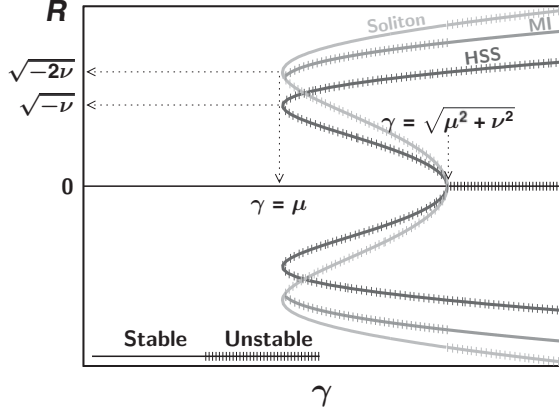


FIG. 2. Bifurcation diagram of the parametrically driven of the solitons [Eqs. (9)] of the parametrically driven damped nonlinear Schrödinger equation. In this diagram, we assume that we are close enough to the curve $\gamma(v) = \sqrt{\mu^2 + v^2}$, so the periodic or chaotic oscillation of the stable soliton is avoided [30]. Discussion about the stability of the homogeneous steady state (HSS) can be found in Ref. [20]. MI refers to the maximum amplitude of the standing waves (ψ^{sw}).

can be formed only if the perturbation falls on its basin of attraction, making a spontaneous formation of the soliton quite difficult. For $\gamma > \sqrt{\mu^2 + v^2}$, both dissipative solitons and the trivial state are unstable. The other nonzero uniform states are represented by HSS, which has the form $\psi_{\pm}^s = R_{\pm}^s e^{i\theta_0}$ such that

$$R_{\pm}^s = \sqrt{-v \pm \sqrt{\gamma^2 + \mu^2}}. \quad (10)$$

These solutions appear via a saddle-node bifurcation, when the injection and dissipation of energy are equal ($\gamma = \mu$), as it is depicted in Fig. 2. Under the influence of dispersive effects ($i\partial_x^2$) the HSSs are unstable by means of a modulational instability. In particular, for the upper branch ψ_+^s , the most unstable mode has a wave number of the form [20,34]

$$k_c = \sqrt{-v + 2\sqrt{\gamma^2 + \mu^2}}. \quad (11)$$

Hence, an expression of the resulting standing wave can be found under the following form of a truncated Fourier expansion,

$$\psi^{sw} = \left\{ \sqrt{-\frac{3v}{5} + \sqrt{\gamma^2 + \mu^2}} + 2\sqrt{-\frac{v}{15}} \cos(k_c X) \right\} e^{i\theta_0}. \quad (12)$$

The solution (12) can then be considered as an approximation of the stable state of Eq. (1) for $\gamma > \sqrt{\mu^2 + v^2}$. Starting from this standing wave, within the region $\mu < \gamma < \sqrt{\mu^2 + v^2}$, the system rapidly develops some instabilities, leading first to the formation of an unstable multipulse state, and then to a cascade of the coalescence process as shown in Fig. 1. The interesting feature of this process is that after a given time one can obtain spontaneously a stable multisoliton state. Then, in this region, the HSS solution is unstable and generates initially a periodic solution, which subsequently becomes unstable, decaying into a multiple-soliton state. Our purpose is to characterize the time scale governing the process under consideration. Clearly, this process is driven by the interaction of pairs of solitons. Thus,

we concentrate our efforts on characterizing this interaction. Indeed, as it can be seen in Fig. 1, only two pulses are involved simultaneously in each coalescence process. This allows us to assume that all of the cascade time law can be derived from the pair interaction law of a two-soliton state.

We have recently studied, experimentally and theoretically, the motion and interaction of the localized excitations in a vertically driven small rectangular water container [26]. Close to the Faraday instability, this system is described by model (1). This model allows us to characterize the pair interaction law between localized excitations. Experimentally we have an excellent agreement with the pair interaction law. In the following, we summarize the main results of this characterization.

A. Analytical approach of isolated solitons pair interaction law

Interaction forces between adjacent localized states are still being studied since the first applications were reported [19,35–38]. The main upshot of these studies is that interaction may be attractive or repulsive depending on the soliton phase. In order to derive quantitatively this interaction in the parametric resonance regime, let us consider a state of two diluted dissipative solitons [Eq. (9)] initially spaced by a distance larger than their typical width. Figure 3 this configuration, where $\Delta(t)$ is the instantaneous distance between the solitons, $\Delta(t)/2$ stands for the *center of mass*, and the *polarity* $\chi = 1$ ($\chi = -1$) corresponds to an in-phase (out-of-phase) interaction. A solution of this state can be written as

$$R(X, \tau) = R_+^0 \left(X - \frac{\Delta(\tau)}{2} \right) + \chi R_+^0 \left(X + \frac{\Delta(\tau)}{2} \right) + \rho(X, \Delta), \quad (13a)$$

$$\theta(X, \tau) = \theta_0 + \varphi(X, \Delta), \quad (13b)$$

where $\rho(X, \Delta)$ and $\varphi(X, \Delta)$ are small correction functions. For simplicity, we place ourselves in the parameter region near the saddle-node bifurcation so $\sqrt{\gamma^2 - \mu^2} \ll \mu \sim \gamma$. In addition, we consider that the solitons are sufficiently separated from each other (diluted) so then we can consider that $\Delta(t)$ varies slowly. Consequently, we have $\ddot{\Delta} \ll \dot{\Delta} \ll 1$ and

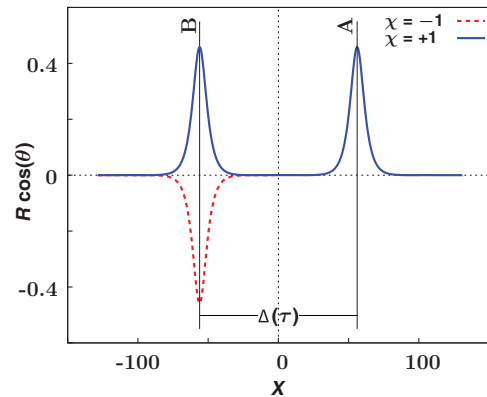


FIG. 3. (Color online) Illustration of a state of a pair of interacting dissipative solitons. The aim of the theoretical study of Sec. III A is the determination of the effective phase and the instantaneous velocity ($\dot{\Delta}$) of solitons.

$\Delta\delta_+^{1/2} \gg 1$. Introducing the ansatz $\psi = R(X, \tau) \exp^{i\theta(X, \tau)}$ in Eq. (1), and using the parameter variation method, we obtained, after a straightforward calculation (see Ref. [26] and details therein), the expression of the phase correction $\varphi(X, \Delta)$ and the instantaneous position $[\Delta(t)]$ of the form

$$\varphi = \dot{\Delta}\Theta(X, \Delta) + O(\sqrt{\gamma - \mu}), \quad (14a)$$

$$\dot{\Delta} = -\frac{3\chi \langle \partial_{z_+} R_{+,+} | R_{+,+}^2 R_{+,-} \rangle}{2\mu \langle \partial_{z_+} R_{+,+} | W\Theta \rangle}, \quad (14b)$$

where

$$\Theta(X, \Delta) \equiv -\int_{-\infty}^X \frac{dX'}{2W^2} \int_{-\infty}^{X'} dy W(\partial_{z_+} R_{+,+} - \chi \partial_{z_-} R_{+,-}), \quad (15a)$$

$$\begin{aligned} \langle \partial_{z_+} R_{+,+} | W\Theta \rangle &= -\int_{-\infty}^{\infty} dz \partial_z R_{+,+} W(z) \int_{-\infty}^X \frac{dX'}{W^2(X')} \\ &\quad \times \int_{-\infty}^{X'} dy W(y) \Lambda(y), \end{aligned} \quad (15b)$$

$$\begin{aligned} \langle \partial_{z_+} R_{+,+} | R_{+,+}^2 R_{+,-} \rangle &= \int_{-\infty}^{\infty} dz \partial_z R_{+,+}(z) R_{+,+}^2 \\ &\quad \times (z) R_{+,-}(z + \Delta), \end{aligned} \quad (15c)$$

$$\begin{aligned} W &= R_+^0(z_+ \equiv X - \Delta/2) + \chi R_+^0(z_- \equiv X + \Delta/2) \\ &= (R_{+,+} + \chi R_{+,-}), \end{aligned} \quad (15d)$$

$$\Lambda(y) \equiv \partial_{z_+} R_{+,+}(y) - \chi \partial_{z_-} R_{+,-}(y). \quad (15e)$$

Integrals (15a)–(15c) can be evaluated taking whichever of the two solitons and considering the asymptotic tendency of one soliton around the other one. For this purpose, let us consider the soliton $R_{+,+}$ (which is represented by curve A in Fig. 3), where the soliton represented by curve B decays exponentially: $R_{+,-}(z + \Delta) \approx 2\sqrt{2}\delta_+ e^{-\delta_+(z+\Delta)}$. Then the integral (15c) can be approximated by

$$\begin{aligned} \langle \partial_{z_+} R_{+,+} | R_{+,+}^2 R_{+,-} \rangle \\ \approx 2\sqrt{2}\delta_+ e^{-\delta_+\Delta} \int_{-\infty}^{\infty} dz \partial_z R_{+,+}(z) R_{+,+}^2(z) e^{-\delta_+z}, \end{aligned} \quad (16)$$

leading finally to the law of soliton pair interaction [26]

$$\dot{\Delta} \approx -\mathcal{R}\chi e^{-\delta_+\Delta}, \quad (17)$$

where

$$\mathcal{R} = \frac{3\sqrt{2}\delta_+ \int_{-\infty}^{\infty} dz \partial_z R_{+,+}(z) R_{+,+}^2(z) e^{-\delta_+z}}{\mu \int_{-\infty}^{\infty} dz \partial_z R_{+,+} W(z) \int_{-\infty}^X \frac{dX'}{W^2(X')} \int_{-\infty}^{X'} dy W(y) \Lambda(y)} \quad (18)$$

is a positive constant. In the limit of large interaction distance, \mathcal{R} explicitly reads

$$\mathcal{R} = \frac{8\delta_+^3}{\mu}. \quad (19)$$

Therefore, the dynamics of a pair of solitons is overdamped and governed by interactions that decrease exponentially with the soliton-soliton distance. This interaction is attractive (repulsive) when solitons are in (out of) phase, that is, for $\chi = 1$ ($\chi = -1$).

For a given initial condition, we can integrate the evolution of the soliton distance, which takes the form

$$\Delta(\tau) = \frac{1}{\delta_+} \ln [\delta_+ \mathcal{R} (\tau_0 - \tau)], \quad (20)$$

where τ_0 is determined by the initial condition by

$$\tau_0 = \chi \frac{e^{\delta_+\Delta_0(\tau=0)}}{\delta_+ \mathcal{R}}, \quad (21)$$

and Δ_0 accounts for both the initial condition and the critical separation distance. For in-phase solitons, formula (20) is valid only for $\tau < \tau_0$. This time is related to the characteristic time of fusion between the two particles. Hence, two dissipative solitons that are in phase follow a logarithmic decrease of their separation distance. Although the above analytical result is valid rigorously for large values of $\Delta(\tau)$, it also gives a quite good approximation at a small interaction length (see, e.g., Fig. 4), where the temporal evolution is to the left-hand side. Figure 4 shows the numerical (red squares) and analytical (blue solid line) reversed temporal evolution of the soliton-soliton distance for an in-phase pair of dissipative solitons. Consequently, the approximate interaction of solitons described by (17) provides a quite good description of the process of solitons interaction. Thus, the dynamics of a soliton pair can be simply reduced to point-particle interactions. Notice that the analytical interaction process described here does not stand for the collapse and subsequent radiation and annihilation of one of the solitons during interaction (the inset of Fig. 4). The study of these processes is still in progress.

B. Experimental measurement of the pair interaction law

Parametric instabilities can take place in a liquid layer that is placed in a vertically forced rectangular container. Nonpropagative solitons described by Eqs. (9) have been reported previously in Refs. [35,39]. This suggests that this could be the proper setup to verify experimentally the interactions among solitons.

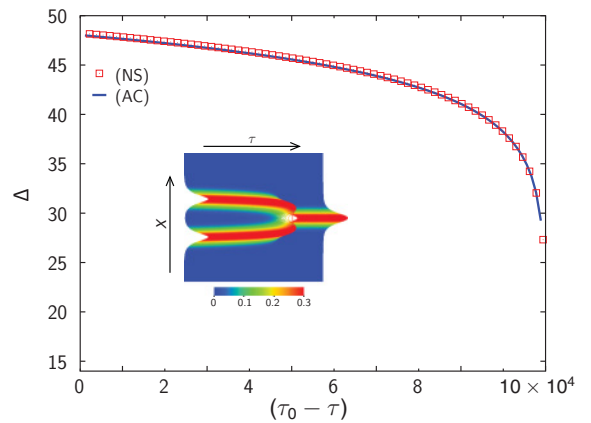


FIG. 4. (Color online) Temporal evolution of soliton separation distance $\Delta(\tau)$ for $\mu = 0.05$, $\gamma = 0.054$, and $\nu = -0.04$. Red squares stand for the numerical simulation of Eq. (1) and the continuous curve is deduced from formula (20). The inset gives the spatiotemporal diagram of the amplitude of ψ .

In Ref. [26] we have recently reported the soliton pair interaction law, studied both theoretically and experimentally. We now briefly explain the experimental setup details and our main results. Experiments were performed on a vertically vibrating plexiglass basin, $L_x = 45$ cm long, $L_z = 9.0$ cm deep, and $L_y = 2.54$ cm wide. The channel is filled with water to a depth $H = 1.5$ cm. Several drops of the wetting agent Kodak Photo-Flo are added to improve wetting and minimize surface pinning on walls. The container is vibrated vertically with an electromechanical shaker (Dynamic Solutions VTS100) fed with a harmonic signal of the form $y(t) = A \sin(\omega t)$ at the frequency $f = \omega/2\pi = 10.2$ Hz. This signal is provided by a function generator (Rigol DG1022) and amplified through a power amplifier. The amplitude A is the experimental control parameter, which is of the order of 0.3 mm. Hence, the typical acceleration container is $\sim 10\%$ the acceleration of gravity. The container acceleration is measured by means of a piezoelectric accelerometer (PCB 340A65) connected to a lock-in-amplifier (SR830) providing a precision of $0.01\%g$. The lower-left-hand inset of Fig. 5 represents an image sequence of a pair of interacting in-phase solitons at different times. The temporal evolution of their separation distance, given by the red filled circles in Fig. 5, fits well with formula (20). Indeed, all the adjusted parameters present relative errors smaller than 6%, for both the in-phase and out-of-phase (upper-right-hand inset of Fig. 5) interactions. These errors are computed from the 95% confidence interval of the adjusted parameters. Therefore, we can conclude that there is excellent agreement between the theoretical description and experimental observations for the interaction law of dissipative solitons.

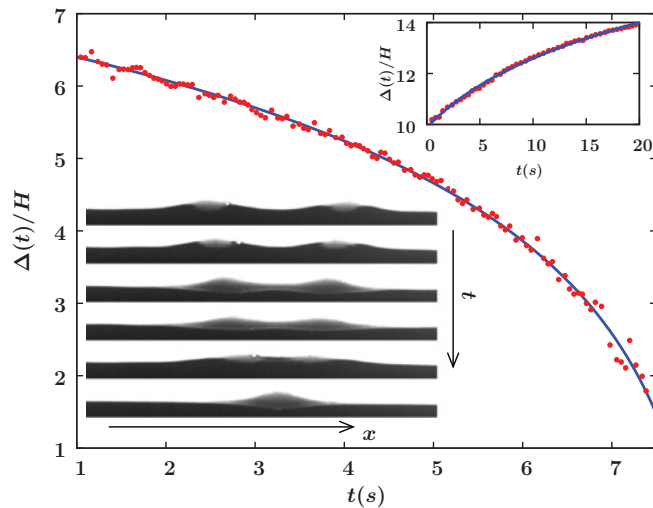


FIG. 5. (Color online) Temporal evolution of separation distance of a pair of in-phase and out-of-phase [inset (b)] solitons in a vertically driven rectangular water container (red filled circles). The fit $\Delta(t) = a \ln[-b(t - t_0)]$ (blue solid line) of the experimental data, motivated by formula (20) gives $a/H = 2.20 \pm 0.04$, $b = 2.7 \pm 0.1 \text{ s}^{-1}$, and $t_0 = 8.20 \pm 0.04 \text{ s}$ for the in-phase solitons and $a/H = 3.00 \pm 0.04$, $b = 4.0 \pm 0.2 \text{ s}^{-1}$, and $t_0 = 6.7 \pm 0.1 \text{ s}$ for the out-of-phase solitons. Inset (b) gives snapshots of the experiment of in-phase soliton interaction at some arbitrary given times.

C. Multisoliton state observations

In order to be able to support a reasonable quantity of solitary waves in our setup, we increased the length and width aspect ratio of the basin $L_x = 50$ cm long, $L_z = 5.0$ cm deep, and $L_y = 2.54$ cm wide. The basin was narrowed by adding two supplementary inner plexiglass walls so the final width is 1.54 cm. The basin was filled up to a depth $H = 2.0$ cm. Nonpropagating solitons are observed when the driving frequency is fixed at ~ 14 Hz and the amplitude is approximately $\Gamma = A\omega^2/g = 0.2$. Faraday waves are also observed in this region of parameters. Small gaps of 5.0 mm width were left between each lateral and supplementary wall. This is done to increase dissipation at the lateral boundaries as this seems to delay the onset of the extended Faraday wave state. This idea was first suggested by Wang and Wei [35].

In contrast to what is observed in the early stages of the simulations of Fig. 1, we have not been able to observe experimentally the onset of a multisoliton state from broken cnoidal waves. Furthermore, the first transverse mode (0, 1), which should give rise to the cnoidal wave state, was not observed either. We believe that this could be due to the *proximity* of different attractors in our physical setup. This competition between modes was already noticed by Wu *et al.* [39]. Even the main direction of motion of one-dimensional (1D) Faraday and solitary waves is different, and the passage from one state to another becomes less difficult. This fact is exacerbated when the aspect ratio is increased as Faraday wave longitudinal modes are contracted in the spectrum. The frequency gaps between the first transverse mode and its two longitudinal closest neighbors become smaller so three attractors are squeezed into a small frequency region. Higher hybrid modes $(n, 1)$ are also compressed near the (0, 1) mode. In the setup, these higher modes usually appear as propagating fronts that resemble a cascade process of creation of out-of-phase successive solitons. Unfortunately, all these effects are out of scope of our numerical simulations. Further research on this subject is still in progress.

Still, multisoliton states can be produced artificially by the creation of many localized structures by hand. It is not difficult to accomplish three-soliton states just by perturbing the water with a paddle in quite separated regions. Solitons must be created in phase and far enough from the wall to avoid pinning. Figure 6(a) shows the interaction between three solitons just after the creation of the last one (notice the logarithmic time axis). The interactions occur by pairs, giving a final one-soliton state.

Despite the difficulty, we had also success in creating four-soliton states. When solitons are created, destabilization into the extended Faraday wave state is much more likely, especially when the distance between neighbor pairs is the same. States characterized by four solitons in phase are harder to obtain than other four solitons states, e.g., $(\uparrow\downarrow\downarrow\uparrow)$, as those reported by Wang *et al.* [35]. Due to the size of our basin, the first interaction occurs very fast. For this reason, we designed a *cage* device that allows the existence of many solitons before letting them interact. The cage allows the basin to be split in several subcells. The plastic separating walls are 0.635 mm thick. They are attached to a rigid structure in such a way that all the walls can be removed at the same time.

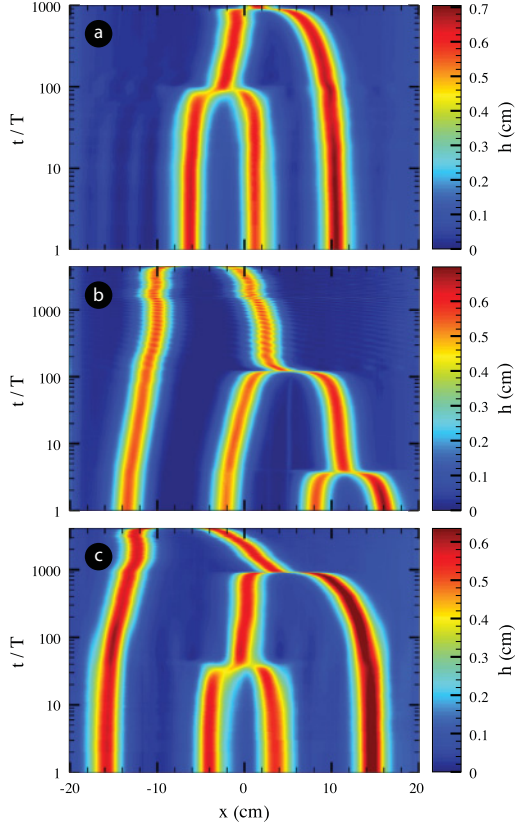


FIG. 6. (Color online) Multisoliton state evolution on the free surface of a $50 \times 1.54 \text{ cm}^2$ rectangular basin filled with water (2 cm depth). The figures show the spatiotemporal diagrams (logarithmic time scale) for three different realizations, unveiling coalescence cascade processes. The images are taken stroboscopically. The forcing frequency is $\nu = 14 \text{ Hz}$ and the amplitudes are (a) $\Gamma = 0.202$ (three solitons) and (b) and (c) $\Gamma = 0.201$ (four solitons).

Solitons could then be created separately in each subcell. After creation, solitons move toward their equilibrium in the center of the subcell. Figures 6(b) and 6(c) show the evolution of the four-soliton state after removing the cage. The picture is the same for the three-soliton interactions: a cascade of pair interactions and a final state consisting of a single solitary wave.

In spite of the fact that the cage can support even eight solitons in phase placed in separate subcells, higher than four stable states could not be observed in our setup. In fact, the layer destabilizes into Faraday waves as soon as the separating wall structures is removed.

Recently, we have reported that soliton motion is affected by basin inclination [40]. Solitonic structures are slowly attracted to a fixed position in the cell following an exponential motion law. This fixed equilibrium position depends on the tilt angle in a very sensitive way. When the basin is correctly aligned, the equilibrium position is located in the center of the basin. If it is not the case, it moves away from the center, and moves farther for steeper tilt angles. Nonparallelism of the fore and back walls would produce a similar outcome on soliton dynamics. We remark on this because this effect breaks spatial invariance in the coalescence process. Thus, any slight deviation on the

walls or the tilt angle would explain the asymmetry arising in the final coalescence process, shown in the spatiotemporal diagrams of Fig. 6. As the supplementary walls added to our setup were very large, we think that small deviations were likely to happen.

Realizations performed with four solitons also show the appearance of strong extended perturbations before the last interaction occurs. Moreover, whenever a pair of solitons coalesces, the other solitons suffer a slight change of behavior. We think that this is due to small adjustments in the driving force, which is actually done at constant power and not constant amplitude. Whenever a soliton is annihilated, the system loses some dissipation related to the decoupling of the soliton momentum. This residual power is then pumped to the whole system and transformed into an amplitude growth.

Our experimental observations show that multisoliton states do exist in a parametrically driven dynamical system. The evolution is characterized by successive fusion processes between solitons that resembles the coalescence cascade observed in the numerical simulations of parametrically driven systems models.

IV. INTERACTION OF A GAS OF SOLITONS

As mentioned in Sec. I, the solitons under consideration appear via a saddle-node bifurcation. Hence, they are generated only if an external perturbation lies within of the basin of attraction. Any spontaneous formation is not possible. For example, in the experiment described above, the dissipative solitons have been generated by a disturbance created by a metallic paddle. In contrast, the nonzero homogeneous steady states emerge spontaneously above the instability threshold, when $-\sqrt{\gamma^2 - \mu^2} \leq \nu \leq \sqrt{\gamma^2 - \mu^2}$ (see Fig. 2). The linear spectrum of this solution shows that it is unstable to a modulational instability with a well-defined wave number close to the bifurcation. Switching the detuning in the stability domain of the nonpropagative soliton, modulational instabilities in turn are unstable and develop a cascade of coalescing collisions (cf. Fig. 1). After a sufficiently long time, this process decays into a multisoliton state which still displays a cascade of soliton pair interactions. In this section, we propose a characterization of the process described above since it can provide a way of spontaneous soliton formation in a parametric forced system.

For this purpose, let us consider now a state of randomly distributed pulses in interaction, as depicted on Fig. 7. Then, using an ansatz for the multiple-soliton solution, which corresponds to a trivial generalization of the ansatz (13), and considering the same type of analysis performed in Sec. III, we can obtain an equation for the position of the i th soliton:

$$\dot{z}_i = \sum_{j=1} (-1)^j \mathcal{R} e^{-\delta(z_i - z_{i-j})} + \mathcal{R} e^{-\delta(z_{i+j} - z_i)}. \quad (22)$$

Then, solitons placed to the left (right) of the i th soliton push the i th soliton to the left (right). As the interaction between the solitons decays exponentially with distance, the evolution will be mainly governed by the closest neighbor interaction. Hence, the above equation can be approximated by

$$\dot{z}_i = -\mathcal{R} e^{-\delta(z_i - z_{i-1})} + \mathcal{R} e^{-\delta(z_{i+1} - z_i)}. \quad (23)$$

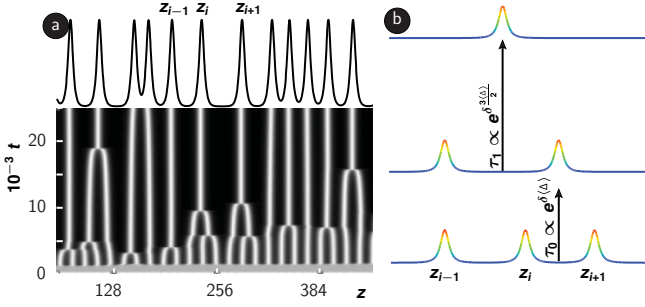


FIG. 7. (Color online) (a) Amplitude spatiotemporal density plot of numerical solution of Eq. (1) for $\mu = 0.05$, $\gamma = 0.053$, and $\nu = -0.03$. The black solid line represents the profile at a given time. (b) Geometrical picture of the three interacting solitons.

Introducing the distance between the left soliton ($i - 1$) and the right one ($i + 1$) as $2\bar{\Delta}$, the time needed to reach the single soliton (*equilibrium*) state is given by $\tau'_0 \propto e^{\delta_+ \bar{\Delta}} + e^{3\delta_+ \bar{\Delta}/2}$, while for the same distance the pair interaction needs $\tau \propto e^{2\delta_+ \bar{\Delta}}$ to reach the single state. Then for large values of $\bar{\Delta}$ the characteristic time to remove the ($i + 2$)th neighbor is approximatively given by $\tau_1 \propto e^{3\delta_+ \bar{\Delta}/2}$. Figure 8 illustrates the geometric properties governing solitons for model (1): the chain of pendula and the easy-plane ferromagnetic spin chain (from top to bottom). These geometric properties are the separation distance Δ of a soliton pair that survives almost to the end of the cascade coalescence process and the average distance $\langle \Delta \rangle$ of a system counting with a large number of solitons. The former is defined by Eq. (20), and the latter by

$$\langle \Delta \rangle = \frac{\sum_{i=0} (z_{i+1} - z_i)}{N}, \quad (24)$$

with N the number dissipative solitons. Consequently, the average distance $\langle \Delta \rangle$ is an implicit function of the time through the quantity N which is a time-dependent function as consequence of the coalescence process [$\langle \Delta \rangle = f(t)$]. Increasing this distance from $\langle \Delta \rangle$ to $\langle \Delta \rangle + \langle \Delta \rangle_0$ involves a dilation of the collision time from t_0 to $t_0 e^{3\delta \langle \Delta \rangle_0 / 2}$. Thus, the dynamics controlled by Eq. (24) is self-similar. Introducing the following self-similar law,

$$z_{i+1} - z_{i-1} \rightarrow z_{i+1} - z_{i-1} + \langle \Delta \rangle_0, \quad (25a)$$

$$t \rightarrow t e^{3\delta \langle \Delta \rangle_0 / 2}, \quad (25b)$$

Eq. (24) is invariant. We get that $f(t)$ must satisfy the condition

$$f(t) + 2\langle \Delta \rangle_0 = f(t e^{3\delta \langle \Delta \rangle_0 / 2}),$$

from which we deduce the temporal evolution of the average distance $\langle \Delta \rangle$ as a coarsening law:

$$\langle \Delta \rangle = \langle \Delta \rangle_0 + \frac{4}{3\delta} \ln t, \quad (26)$$

where $\langle \Delta \rangle_0$ is an arbitrary constant depending on the initial condition. Therefore, for a dilute gas of solitons the average separation between solitons grows logarithmically with time.

Given the generic nature of model (1), one expects that the coarsening law is valid for a variety of parametrically

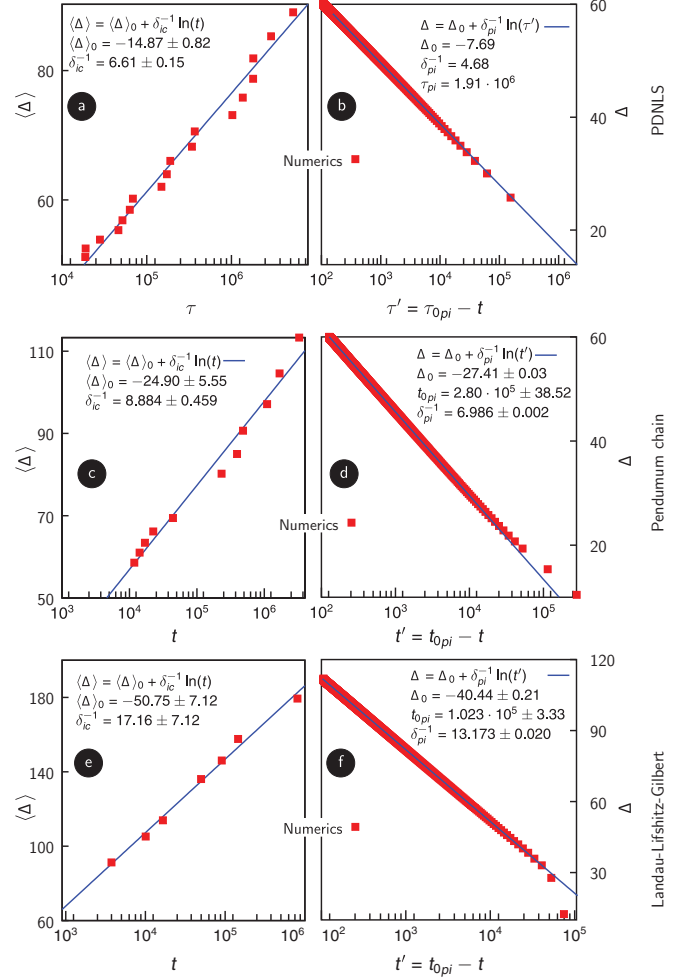


FIG. 8. (Color online) Left-hand column: Average soliton-soliton distance evolution for the coalescence cascade. Right-hand column: The separation distance for a soliton pair that survives almost to the end of the cascade coalescence process. Squares represent the numerical results and the blue solid lines give the nonlinear interpolations with respect to our analytical predictions, Eqs. (20) and (26). The numerical results obtained from (a), (b) the PDNLS equation ($\mu = 0.05$, $\gamma = 0.053$, and $\nu = -0.03$), (c), (d) the pendulum chain ($\gamma = 0.21$, $\mu = 0.1$, $\nu = -0.03$), and (e), (f) the ferromagnetic spin chain ($H_0 = 0.2$, $h_1 = 0.044$, $\beta = 4.8$, $\alpha = 0.02$, $\nu = -0.03$).

forced systems exhibiting solitons. In Fig. 8, we contrast our analytical prediction with the results of numerical simulations of the parametrically driven damped nonlinear Schrödinger equation (PDNLS), the vertically driven pendula chain, and a forced ferromagnetic spin chain [Landau-Lifshitz-Gilbert (LLG) equation]. As it can be seen in Fig. 8, both logarithmic law and its predicted scaling factor are in a gratifying agreement with our analytical results. Indeed, the ratio between the logarithmic growth of the average soliton-soliton distance and that of the decay of the pair interaction are 1.33 (PDNLS), 1.4 (pendulum chain), and 1.51 (spin chain), while the predicted value is 1.33. Hence, the cascade of coalescence that seems complex can be well described by the interaction of a soliton pair. We emphasize here that although the interaction of pair of solitons is valid for remote solitons and

does not render to the collapse process, it provides a good tool to understand a dynamical process that could generate spontaneously dissipative solitons in any parametrically driven system.

Even though several coalescence processes could be studied experimentally in the vertically driven channel with water, the characterization of a coarsening law cannot be verified using the current setup. This would require a large number of solitons, at least 100, which is not achievable with the present setup.

V. CONCLUSIONS

Nonlinear dissipative and dispersive systems under parametric forcing exhibit a great variety of spatiotemporal coherent structures. Over and above their difference from the point of view of the dynamical behavior, these structures also differ in the way they are excited. For instance, since the Faraday instabilities rise spontaneously above a given threshold, the solitary wave needs an external perturbation that is more or less energetic. Therefore, the localized structures cannot appear spontaneously starting from the basic state, although their threshold is attained. In this paper, we have investigated, both theoretically and experimentally, the way to generate spontaneously parametrically sustained solitary structures. In fact, we have observed numerically that a homogeneous steady state can be spontaneously excited when driving a system very close to the parametric resonance. Then, switching to the

region of existence of the solitary waves, this homogeneous state is unstable to a periodic one (cnoidal wave), which in turn develops rapidly, displaying an irregular cascade of a coalescence process leading to a diluted gas of solitons. We show that the time scale of the formation of this nonpropagative multisoliton state obeys a self-similar law, which has been derived from the two isolated soliton interaction laws. A detailed analytical calculation of this pair interaction law has also been proposed. The model is able to reproduce the experimental measurements carried out in a vertically driven Newtonian fluid in a rectangular container. We also report the existence of multisoliton states in the same setup. This state evolves to a one-soliton state through a cascade of coalescence processes driven by pair interactions.

Despite the large number of simplifications to derive the coarsening law that is valid in the limit of dilute soliton gas, we have compared this prediction with several models, such as the parametrically driven damped nonlinear Schrödinger equation, a vertically driven chain of pendula, and a parametric forced magnetic wire, where we found excellent agreement.

ACKNOWLEDGMENTS

The simulation software *DimX* developed at INLN, France, has been used for all the numerical simulations. M.G.C. acknowledges the financial support of Fondecyt Grant No. 1090045. N.M. and M.G.C acknowledge the financial support of Anillo ACT 127. L.G. thanks CONICYT for support.

-
- [1] G. Nicolis and I. Prigogine, *Self-Organization in Non Equilibrium Systems* (Wiley, New York, 1977).
 - [2] L. M. Pismen *Patterns and Interfaces in Dissipative Dynamics*, Springer Series in Synergetics (Springer, Berlin, 2006).
 - [3] M. Cross and H. Greenside, *Pattern Formation and Dynamics in Nonequilibrium Systems* (Cambridge University Press, New York, 2009).
 - [4] M. C. Cross and P. C. Hohenberg, *Rev. Mod. Phys.* **65**, 851 (1993).
 - [5] Igor S Aranson and Lorenz Kramer, *Rev. Mod. Phys.* **74**, 99 (2002).
 - [6] A. C. Newell, *Solitons in Mathematics and Physics* (SIAM, Philadelphia, 1985).
 - [7] J. Swift and P. C. Hohenberg, *Phys. Rev. A* **15**, 319 (1977).
 - [8] C. Sulem and P.-L. Sulem, *The Nonlinear Schrödinger Equation: Self-Focusing and Wave Collapse* (Springer, New York, 1999).
 - [9] J. D. Murray, *Mathematical Biology* (Springer, Berlin, 1989).
 - [10] M. I. Rabinovich, P. D. Weidman, and A. B. Ezersky, *The Dynamics of Pattern* (World Scientific, Singapore, 2000).
 - [11] A. Pikovsky, M. Rosenblum, and J. Kurths, *Synchronization: A Universal Concept in Nonlinear Sciences* (Cambridge University Press, New York, 2001).
 - [12] L. D. Landau and E. M. Lifshitz, *Course of Theoretical Physics Vol. I: Mechanics*, 3rd ed. (Butterworth-Heinemann, Burlington, MA, 1982).
 - [13] M. Faraday, *Philos. Trans. R. Soc. London* **121**, 299 (1831).
 - [14] J. W. Miles, *J. Fluid Mech.* **148**, 451 (1984); W. Zhang and J. Viñals, *Phys. Rev. Lett.* **74**, 690 (1995); X. Wang and R. Wei, *Phys. Rev. E* **57**, 2405 (1998).
 - [15] I. V. Barashenkov and E. V. Zemlyanaya, *Phys. Rev. Lett.* **83**, 2568 (1999).
 - [16] K. Kumar and K. M. S. Bajaj, *Phys. Rev. E* **52**, R4606 (1995).
 - [17] M. Silber and M. R. E. Proctor, *Phys. Rev. Lett.* **81**, 2450 (1998).
 - [18] I. S. Aranson, L. S. Tsimring, and V. M. Vinokur, *Phys. Rev. E* **59**, R1327 (1999).
 - [19] S. Longhi, *Phys. Rev. E* **53**, 5520 (1996).
 - [20] M. G. Clerc, S. Coulibaly, and D. Laroze, *Phys. Rev. E* **77**, 056209 (2008); *Int. J. Bifurcation Chaos Appl. Sci. Eng.* **3525** (2009).
 - [21] M. G. Clerc, S. Coulibaly, and D. Laroze, *Physica D* **239**, 72 (2010).
 - [22] M. G. Clerc, S. Coulibaly, and D. Laroze, *Int. J. Bifurcation Chaos Appl. Sci. Eng.* **19**, 2717 (2009).
 - [23] M. Clerc, P. Couillet, and E. Tirapegui, *Phys. Rev. Lett.* **83**, 3820 (1999); *Int. J. Bifurcation Chaos Appl. Sci. Eng.* **11**, 591 (2001); *Opt. Commun.* **166**, 159 (1999); *Phys. Lett. A* **287**, 198 (2001); *Prog. Theor. Phys. Suppl.* **139**, 337 (2000).
 - [24] S. Fauve and O. Thual, *Phys. Rev. Lett.* **64**, 282 (1990).
 - [25] X. Wang, *Physica D* **154**, 337 (2001).
 - [26] M. G. Clerc, S. Coulibaly, N. Mujica, R. Navarro, and T. Sauma, *Phil. Trans. R. Soc. A* **367**, 3213 (2009).
 - [27] V. I. Arnold, *Mathematical Methods of Classical Mechanics*, 2nd ed. (Springer, Berlin, 1989), p. 113.

- [28] B. Denardo, B. Galvin, A. Greenfield, A. Larraza, S. Putterman, and W. Wright, *Phys. Rev. Lett.* **68**, 1730 (1992).
- [29] J. N. Kutz, W. L. Kath, R. D. Li, and P. Kumar, *Opt. Lett.* **18**, 802 (1993).
- [30] I. V. Barashenkov, M. M. Bogdan, and V. I. Korobov, *Europhys. Lett.* **15**, 113 (1991).
- [31] N. V. Alexeeva, I. V. Barashenkov, and G. P. Tsironis, *Phys. Rev. Lett.* **84**, 3053 (2000).
- [32] N. Grønbech-Jensen, Y. S. Kivshar, and M. R. Samuelsen, *Phys. Rev. B* **47**, 5013 (1993).
- [33] H. J. Mikeska, *J. Phys. C* **11**, L29 (1978).
- [34] S. Longhi and A. Geraci, *Appl. Phys. Lett.* **67**, 3060 (1995).
- [35] X. Wang and R. Wei, *Phys. Rev. Lett.* **78**, 2744 (1997); *Phys. Lett. A* **227**, 55 (1997).
- [36] J. P. Gordon, *Opt. Lett.* **8**, 596 (1983).
- [37] N. J. Smith, W. J. Firth, K. J. Blow, and K. Smith, *Opt. Lett.* **19**, 16 (1994).
- [38] A. Mecozzi, W. L. Kath, P. Kumar, and C. G. Goedde, *Opt. Lett.* **19**, 2050 (1994).
- [39] J. Wu, R. Keolian, and I. Rudnick, *Phys. Rev. Lett.* **52**, 1421 (1984).
- [40] L. Gordillo, T. Sauma, Y. Zárate, I. Espinoza, M. G. Clerc, and N. Mujica, *Eur. Phys. J. D* **62**, 39 (2011).